HHS Public Access

Author manuscript

Exp Gerontol. Author manuscript; available in PMC 2021 November 01.

Published in final edited form as:

Exp Gerontol. 2020 November ; 141: 111078. doi:10.1016/j.exger.2020.111078.

Txn2 haplodeficiency does not affect cochlear antioxidant defenses or accelerate the progression of cochlear cell loss or hearing loss across the lifespan

Mi-Jung Kim[a], **Chul Han**[a], **Karessa White**[a], **Hyo-Jin Park**[a], **Dalian Ding**[b], **Kevin Boyd**[a], **Christina Rothenberger**[a], **Upal Bose**[a], **Peter Carmichael**[a], **Paul J. Linser**[c], **Masaru Tanokura**[d], **Richard Salvi**[b], **Shinichi Someya**[a,*]

[a]Department of Aging and Geriatric Research, University of Florida, Gainesville, FL, USA

[b]Center for Hearing and Deafness, State University of New York at Buffalo, NY, USA

[c]Whitney Laboratory, University of Florida, St Augustine, FL, USA

[d]Department of Applied Biological Chemistry, University of Tokyo, Yayoi, Tokyo, Japan

Abstract

Thioredoxin 2 (TXN2) is a small redox protein found in nearly all organisms. As a mitochondrial member of the thioredoxin antioxidant defense system, TXN2 interacts with peroxiredoxin 3 (PRDX3) to remove hydrogen peroxide. Accordingly, TXN2 is thought to play an important role in maintaining the appropriate mitochondrial redox environment and protecting the mitochondrial components against oxidative stress. In the current study, we investigated the effects of *Txn2* haplodeficiency on cochlear antioxidant defenses, auditory function, and cochlear cell loss across the lifespan in wild-type (WT) and *Txn2* heterozygous knockout (*Txn2*$^{+/-}$) mice backcrossed onto CBA/CaJ mice, a well-established model of age-related hearing loss. *Txn2*$^{+/-}$ mice displayed a 58% decrease in TXN2 protein levels in the mitochondria of the inner ears compared to WT mice. However, *Txn2* haplodeficiency did not affect the thioredoxin or glutathione antioxidant defense in both the mitochondria and cytosol of the inner ears of young mice. There were no differences in the levels of mitochondrial biogenesis markers, mitochondrial DNA content, or oxidative DNA and protein damage markers in the inner ears between young WT and *Txn2*$^{+/-}$ mice. In a mouse inner ear cell line, knockdown of *Txn2* did not affect cell viability under hydrogen peroxide

*Corresponding author: Department of Aging and Geriatric Research, University of Florida, Gainesville, Florida 32610, USA. Tel: 352-294-5167; fax: 352-294-5058; someya@ufl.edu.

Author contributions

Mi-Jung Kim: investigation, formal analysis, validation, writing - original draft investigation **Chul Han:** investigation, formal analysis **Karessa White:** investigation, formal analysis **Hyo-Jin Park:** investigation, formal analysis **Dalian Ding:** investigation **Kevin Boyd:** investigation **Christina Rothenberger**: investigation **Upal Bose:** investigation **Peter Carmichael:** investigation **Paul J. Linser:** investigation **Masaru Tanokura:** supervision, writing - review & editing, funding acquisition **Richard Salvi:** formal analysis, supervision, writing - review & editing **Shinichi Someya:** conceptualization, resources, writing - review & editing, supervision, project administration, funding acquisition.

Conflict of interest

The authors declare that there are no conflicts of interest.

treatment. Consistent with the tissue and cell line results, there were no differences in hair cell loss or spiral ganglion neuron density between WT and *Txn2*$^{+/-}$ mice at 3–5 or 23–25 months of age. Furthermore, *Txn2* haplodeficiency did not affect auditory brainstem response threshold, wave I latency, or wave I amplitude at 3–5, 15–16, or 23–25 months of age. Therefore, *Txn2* haplodeficiency does not affect cochlear antioxidant defenses, accelerate degeneration of cochlear cells, or affect auditory function in mice across the lifespan.

Keywords

mitochondria; antioxidant defense; oxidative stress; cochlea; hearing loss

1. Introduction

Thioredoxin (TXN) is a small redox protein with a mass of 12 kDa and a dithiol/disulfide in the conserved active site Cys-Gly-Pro-Cys and found in nearly all organisms (Holmgren, 1985; Arner and Holmgren, 2000; Powis and Montfort, 2001; Lillig and Holmgren, 2007; Lu and Holmgren, 2014). The reduced form of TXN catalyzes the reduction of disulfide bonds in substrate proteins, while the oxidized form of TXN is reversibly reduced by NADPH-dependent thioredoxin reductase (TXNRD). The diversity of substrates allows TXN to function in multiple biological pathways, including DNA synthesis (Holmgren, 1989), regulation of transcription factors (Schenk *et al.*, 1994; Hirota *et al.*, 1999), regulation of apoptosis (Saitoh *et al.*, 1998), immunomodulation (Silberstein *et al.*, 1993; Nakamura *et al.*, 1997; Bertini *et al.*, 1999), and antioxidant defense (Zhang *et al.*, 1997; Kang *et al.*, 1998; Chae *et al.*, 1999). It is well documented that the majority of intracellular reactive oxygen species (ROS) are generated as a by-product of mitochondrial respiration metabolism during the generation of ATP (Balaban *et al.*, 2005; Lin and Beal, 2006; Cui *et al.*, 2012). These ROS include superoxide ($\bullet O_2^-$) and hydrogen peroxide (H_2O_2). An elaborate antioxidant system has evolved to control the cytotoxic effects of those ROS. The system includes superoxide dismutase (SOD), catalase (CAT), glutathione peroxidase (GPX), and peroxiredoxin (PRDX), and small-molecule antioxidants such as glutathione and TXN (Evans and Halliwell, 1999; Birben *et al.*, 2012). In mitochondria, there are two major players in the thioredoxin antioxidant defense system: TXN2 and TXNRD2. When TXN2 is in a reduced state, the two active site cysteines form a dithiol group that catalyzes the reduction of disulfide bonds in a number of oxidized proteins and interacts with peroxiredoxin 3 (PRDX3), a member of the peroxidase family, to remove H_2O_2, which is decomposed into water. NADPH-dependent TXNRD2 then regenerates reduced TXN2 from oxidized TXN2 (Lu and Holmgren, 2014). The thioredoxin system is thought to work with other antioxidant systems such as the glutathione antioxidant defense system to protect the mitochondrial components from oxidative stress (Lu and Holmgren, 2014; Ribas *et al.*, 2014). An increasing body of evidence indicates that the mitochondrial antioxidant defense systems do not keep pace with the age-related increase in ROS production, and thus the balance between antioxidant defense and ROS production shifts progressively toward a more pro-oxidant state during aging (Rebrin and Sohal, 2008).

Age-related hearing loss (AHL) is the most common form of hearing impairment in older adults and is associated with loss of sensory hair cells, spiral ganglion neurons, and/or stria vascularis cells in the cochlea of the inner ears (Gates and Mills, 2005; Yamasoba *et al.*, 2013). A large body of evidence indicates that oxidative stress and associated mitochondrial dysfunction contribute to the development of AHL (Kokotas *et al.*, 2007; Someya and Prolla, 2010; Yamasoba *et al.*, 2013). This idea is supported by the observations that oxidative damage to DNA and protein increases with age in the cochlea of laboratory animals (Jiang *et al.*, 2007; Someya *et al.*, 2009). Similarly, lack of SOD1 enhances age-related cochlear hair cell loss (McFadden *et al.*, 1999), while overexpression of mitochondrially targeted catalase (MCAT) extends lifespan (Schriner *et al.*, 2005), decreases oxidative DNA damage in the cochlea, and delays the onset of AHL in mice (Someya *et al.*, 2009). In cultured cells, overexpression of *TXN2* in human embryo kidney 293 cells results in increased mitochondrial membrane potential and decreased etoposide-induced cell death (Damdimopoulos *et al.*, 2002). Overexpression of *TXN2* in human 143B osteosarcoma cells also leads to increased cell viability under treatment with tert-butylhydroperoxide (Chen *et al.*, 2002). Moreover, chicken DT40 B cells deficient for *TXN2* display increased intracellular ROS and apoptosis (Tanaka *et al.*, 2002). In flies, null mutations in *Txn2* shorten the lifespan, while overexpression of *Txn2* increases tolerance to H_2O_2 (Svensson and Larsson, 2007). In mice, a complete loss of the *Txn2* gene results in embryonic lethality at E10.5–12.5 associated with anterior neural tube defect and massive apoptosis (Nonn *et al.*, 2003), while *Txn2* heterozygous knockout (*Txn2*$^{+/-}$) mice display increased oxidative damage to DNA, protein, and lipid, decreased activity of the electron transport chain complexes, and decreased ATP production in the liver (Perez *et al.*, 2008). However, the roles of TXN2 in maintaining cochlear antioxidant defenses and protecting aged cochlear tissues against oxidative stress are largely unknown. Therefore, we investigated the effects of *Txn2* haplodeficiency on cochlear antioxidant defenses, auditory function, and cochlear cell loss across the lifespan in wild-type (WT) and *Txn2* heterozygous knockout (*Txn2*$^{+/-}$) mice backcrossed onto CBA/CaJ mice, a normal-hearing strain which exhibits AHL beginning at 17–20 months of age (Zheng *et al.*, 1999; Noben-Trauth *et al.*, 2003; Ohlemiller, 2006; Han and Someya, 2013).

2. Materials and methods

2.1. Animals

Txn2$^{+/-}$ mice were obtained from Taconic Biosciences (https://www.taconic.com/knockout-mouse/txn2-trapped). CBA/CaJ mice were purchased from the Jackson Laboratory (https://www.jax.org/strain/000654). *Txn2*$^{+/-}$ mice were backcrossed onto CBA/CaJ mice for four generations. N4 heterozygous *Txn2*$^{+/-}$ mice were subsequently intercrossed to generate WT and *Txn2*$^{+/-}$ littermates. No *Txn2*$^{-/-}$ pups were born, consistent with the previous report that homozygous *Txn2*$^{-/-}$ mice are embryonic lethal (Nonn *et al.*, 2003). Both male and female WT and *Txn2*$^{+/-}$ mice were used in the current study. All animal experiments were conducted under protocols approved by the University of Florida Institutional Animal Care and Use Committee.

2.2. Genotyping

2.2.1. Txn2 genotyping— *Txn2*$^{+/-}$ males were mated with *Txn2*$^{+/-}$ females and their offspring were genotyped by PCR with DNA isolated from the tails of these pups at weaning. Primer sequences and cycling conditions for PCR were as follows:

LTR2 5'-AAATGGCGTTACTTAAGCTAGCTTGC-3';

TF1252 forward 5'-AACCTACCTGTTGCCCTGAGTATGG-3';

TF1252 reverse 5'-GAATTCTGGAATAATGAGGTGTTGG-3';

94 °C for 4 min; 10 cycles of 94 °C for 15 sec, 65 °C for 30 sec decreasing 1 °C/cycle, 72 °C for 30 sec; 30 cycles of 94 °C for 15 sec, 55 °C for 30 sec, 72 °C for 30 sec. The TF1252 forward and TF1252 reverse primers were used to detect the wild-type allele, while the LTR2 and TF1252 reverse primers were used to detect the mutant allele. PCR products were separated on 2% agarose gel. The expected band sizes for the wild-type and mutant alleles were 478 and 281 bps, respectively.

2.2.2. Cdh23 genotyping—The *Txn2*$^{+/-}$ mice provided by Taconic Biosciences were originally developed in the mixed 129S5 × C57BL/6J background (https://www.taconic.com/knockout-mouse/txn2-trapped). The C57BL/6J mouse strain is homozygous for the age-related hearing loss (AHL)-susceptibility allele (*Cdh23*^{753A}) and AHL in C57BL/6 mice is early onset, caused primarily by the G to A substitution at nucleotide position 753 of the *Cdh23* (cadherin 23) gene (Zheng *et al.*, 1999; Noben-Trauth *et al.*, 2003; Ohlemiller, 2006; Han and Someya, 2013). To remove this mutation, the *Txn2*$^{+/-}$ mice were backcrossed for four generations onto the CBA/CaJ mouse strain, a normal-hearing strain that is homozygous for the AHL-resistance allele (*Cdh23*^{753G}) and exhibits AHL beginning at 17–20 months of age (Zheng *et al.*, 1999; Noben-Trauth *et al.*, 2003; Ohlemiller, 2006; Han and Someya, 2013). To confirm that N4 WT and *Txn2*$^{+/-}$ mice have the same wild-type *Cdh23* genotype (*Cdh23*$^{753G/753G}$), we isolated DNA from the tails of these mice, amplified by PCR, and then sequenced the region of DNA containing the 753rd nucleotide in the *Cdh23* gene. Primer sequences and cycling conditions for PCR were as follows:

Cdh23 forward 5'-GATCAAGACAAGACCAGACCTCTGTC-3';

Cdh23 reverse 5'-GAGCTACCAGGAACAGCTTGGGCCTG-3';

95 °C for 2 min; 35 cycles of 95 °C for 30 sec, 60 °C for 1 min, 72 °C for 1 min; 72 °C for 5 min. The expected size of the PCR product was 360 bps. The *Cdh23* gene in three WT and three *Txn2*$^{+/-}$ mice was sequenced. All the mice examined had the same wild-type *Cdh23* genotype (*Cdh23*$^{753G/753G}$).

2.3. Body weight

The body weights of male and female WT and *Txn2*$^{+/-}$ mice were measured every month from 4 months of age until 24 months of age. We used 7–12 mice per group for body weight measurement.

2.4. Cochlear histology

2.4.1. Sample preparation—Mice were sacrificed by cervical dislocation. Temporal bones were excised from the head and divided into cochlear and vestibular parts as previously described (Park *et al.*, 2019; Kim *et al.*, 2019). For cochleograms, the excised cochleae were fixed in 10% formalin for 1 d. To make paraffin-embedded cochlear sections, the excised cochleae were fixed in 4% paraformaldehyde in PBS for 1 d, decalcified in 10% EDTA, pH 7.4, in PBS for 5–7 d, and embedded in paraffin. The paraffin-embedded cochlear specimens were sliced into 5 μm sections, mounted on glass slides, and stained with haematoxylin and eosin (H&E). H&E-stained cochlear sections were used for SGN counting. Unstained cochlear sections were used for immunohistochemistry.

2.4.2. Immunohistochemistry—For confocal-based immunostaining of TXN2, the cochlear sections were deparaffinized, rehydrated, and subjected to antigen retrieval as previously described (White *et al.*, 2017; Park *et al.*, 2019). The sections were then incubated with the anti-TXN2 antibody (Abcam, ab71262) overnight at 4 °C. The following day, the slides were washed and incubated with fluorophore-conjugated secondary antibodies (Jackson ImmunoResearch Laboratories) for 2 h at 37 °C. Nuclei were counterstained with DAPI (4′,6-diamidino-2-phenylindole, Thermo Fisher Scientific). Immunostained samples were imaged using the Leica SP5 laser scanning confocal microscope (Leica Microsystems).

2.4.3. Cochleogram—Inner hair cells (IHCs) and three rows of outer hair cells (OHCs) were counted over 0.24 mm intervals along the entire length of the cochlea under a microscope at 400X magnification as previously described (Ding *et al.*, 2013; Ding *et al.*, 2016). The counting results were then entered into a custom software designed to compute a cochleogram that shows percentage of missing IHCs and OHCs as a function of percentage distance from the apex of the cochlea. The frequency-place map for mouse cochlea (Muller *et al.*, 2005; Ding *et al.*, 2016) was shown on the abscissa in Fig. 4A–B. We used 3–5 mice per group for cochleogram.

2.4.4. SGN counting—Spiral ganglion neurons (SGNs) were counted in the apical and basal regions of the H&E-stained cochlear sections using a 40X objective of a Leica DM3000 microscope (Leica Microsystems) and ImageJ software (National Institutes of Health) as previously described (Park *et al.*, 2019; Kim *et al.*, 2019). SGN density was measured as the number of SGNs per mm^2. Three to nine sections of the apical and basal turns were evaluated in one cochlea per mouse. We used 3 mice per group for SGN counting.

2.5. Isolation of nuclei, mitochondria, and cytosol

Differential centrifugation was performed as previously described (Han *et al.*, 2017; White *et al.*, 2018) to obtain crudely purified nuclear, mitochondrial, and cytosolic fractions. Mouse inner ear tissues were harvested and homogenized using a 7 ml Dounce tissue grinder (Wheaton) followed by further disruption using a 1 ml syringe with 27 G × 1/2 in needle (BD). Homogenization buffer contained 10 mM Tris-HCl, 1 mM EDTA, pH 7.4, 320 mM sucrose, and protease inhibitors. The homogenate was incubated on ice and then centrifuged

at 720 × g for 5 min at 4 °C to obtain a nuclear pellet. The supernatant was further centrifuged at 12000 × g for 10 min at 4 °C to obtain a mitochondrial pellet and the supernatant (cytosolic fraction). The nuclear and mitochondrial pellets were resuspended in lysis buffer (50 mM Tris-HCl, 250 mM NaCl, 1% NP-40, pH 7.4, and protease inhibitors), incubated on ice, and then centrifuged at 12000 × g for 10 min at 4 °C to obtain each supernatant (nuclear and mitochondrial fractions).

2.6. Western blot

Twenty micrograms of protein from each sample was fractionated by SDS-PAGE and transferred to nitrocellulose membranes (Bio-Rad Laboratories). The membranes were incubated with primary antibodies followed by horseradish peroxidase-conjugated secondary antibodies. Chemiluminescent detection reagents (GE Healthcare Life Sciences) were used to visualize proteins. Band intensities were quantified using ImageJ software (National Institutes of Health) and the levels of each protein were normalized by loading controls. Primary antibodies used were as follows: anti-TXN2 (R&D Systems, MAB5765), anti-TXN1 (Abcam, ab26320), anti-Lamin B1 (used as a nuclear loading control, Abcam, ab16048), anti-VDAC (voltage-dependent anion channel, used as a mitochondrial loading control, Cell Signaling Technology, 4866), and anti-GAPDH (glyceraldehyde 3-phosphate dehydrogenase, used as a cytosolic loading control, Sigma-Aldrich, G9545). Secondary antibodies were used as follows: anti-mouse (GE Healthcare Life Sciences, NA931V) and anti-rabbit (GE Healthcare Life Sciences, NA934V).

2.7. ABR hearing test

Auditory brainstem response (ABR) hearing tests were performed using a TDT Auditory Workstation (Tucker-Davis Technologies) as previously described (Park *et al.*, 2019; Kim *et al.*, 2019). Mice were anesthetized with ketamine (100 mg/kg) and xylazine (10 mg/kg) by intraperitoneal injection. Subdermal needle electrodes were placed at the vertex (active), ipsilateral ear (reference), and contralateral ear (ground). ABR thresholds were measured with a tone burst stimulus at 4, 8, 16, 32, 48, and 64 kHz. At each frequency, the sound level was reduced in 5–10 dB SPL steps from 90 to 10 dB SPL. A hearing threshold was determined as the lowest sound level that produced a noticeable ABR. Latencies and amplitudes for ABR wave I were also measured with a click stimulus of 100 dB peak SPL. A wave I latency was determined by measuring the amount of time elapsed from the onset of the stimulus to the highest value (peak) of the first ABR wave. A wave I amplitude was determined by measuring the voltage difference between the highest value (peak) and the lowest value (trough) of the first ABR wave. We used 6–10 mice per group for ABR threshold, wave I latency, and wave I amplitude measurements.

2.8. mRNA expression of genes involved in the thioredoxin and glutathione antioxidant defense systems and mitochondrial biogenesis

Total RNA was isolated from mouse inner ear tissues using the NucleoSpin RNA kit (Macherey-Nagel) according to the manufacturer's instructions. cDNA was synthesized from the total RNA using the SuperScript III First-Strand Synthesis System (Thermo Fisher Scientific) according to the manufacturer's instructions. Quantitative PCR was performed to measure mRNA levels of genes involved in the thioredoxin and glutathione systems and

mitochondrial biogenesis. Relative gene expression was normalized to *Gapdh*. The reactions were performed using the TaqMan Gene Expression Master Mix and Assays (Thermo Fisher Scientific) on the Applied Biosystems 7300 Real-Time PCR System (Thermo Fisher Scientific) according to the manufacturer's instructions. The following TaqMan Assays were used: *Txn1* (thioredoxin 1, Mm00726847_s1), *Txn2* (thioredoxin 2, Mm00444931_m1), *Txnrd1* (thioredoxin reductase 1, Mm00443675_m1), *Txnrd2* (thioredoxin reductase 2, Mm00496766_m1), *Prdx2* (peroxiredoxin 2, Mm04208213_g1), *Prdx3* (peroxiredoxin 3, Mm00545848_m1), *Gsr* (glutathione reductase, Mm00439154_m1), *Gpx1* (glutathione peroxidase 1, Mm00656767_g1), *Gss* (glutathione synthetase, Mm00515065_m1), *Gclc* (glutamate-cysteine ligase, catalytic subunit, Mm00802655_m1), *Gclm* (glutamate-cysteine ligase, modifier subunit, Mm01324400_m1), *Tfam* (transcription factor A, mitochondrial, Mm00447485_m1), *Ppargc1a* (peroxisome proliferative activated receptor, gamma, coactivator 1 alpha, Mm01208835_m1), *Nrf1* (nuclear respiratory factor 1, Mm01135606_m1), and *Gapdh* (glyceraldehyde-3-phosphate dehydrogenase, used as a housekeeping gene, Mm99999915_g1).

2.9. Antioxidant enzyme activity

2.9.1. TXNRD activity—The activities of thioredoxin reductase (TXNRD) were measured in nuclear, mitochondrial, and cytosolic fractions isolated from mouse inner ear tissues using the Thioredoxin Reductase Assay Kit (Sigma-Aldrich) according to the manufacturer's instructions. In brief, 10 μl of each fraction was added to the wells of a 96 well plate and then 184 μl of the mixture containing 180 μl of the Working Buffer (100 mM potassium phosphate, 10 mM EDTA, and 0.24 mM NADPH) and 4 μl of either the 1x Assay Buffer (100 mM potassium phosphate, pH 7.0, and 10 mM EDTA) or the Thioredoxin Reductase Inhibitor Solution was added to each well. The reaction was started by adding 6 μl of 100 mM DTNB (5,5'-dithiobis(2-nitrobenzoic acid)). The absorbance was read at 405 nm every 10 sec for 2 min in the SpectraMax 340 microplate reader (Molecular Devices) to calculate the activity. All samples were run in duplicate.

2.9.2. GPX activity—The activities of glutathione peroxidase (GPX) were measured in nuclear, mitochondrial, and cytosolic fractions isolated from mouse inner ear tissues using the Glutathione Peroxidase Cellular Activity Assay Kit (Sigma-Aldrich) according to the manufacturer's instructions. In brief, 30 μl of each fraction was added to the wells of a 96 well plate and then 168 μl of the mixture containing 158 μl of the Assay Buffer (50 mM Tris-HCl, pH 8.0, and 0.5 mM EDTA) and 10 μl of the NADPH Assay Reagent (5 mM NADPH, 42 mM reduced glutathione, and 10 units/ml glutathione reductase) was added to each well. The reaction was started by adding 2 μl of 30 mM *t*-Bu-OOH. The absorbance was read at 340 nm every 10 sec for 2 min in the SpectraMax 340 microplate reader (Molecular Devices) to calculate the activity. All samples were run in duplicate.

2.9.3. SOD activity—The activities of superoxide dismutase (SOD) were measured in mitochondrial and cytosolic fractions isolated from mouse inner ear tissues using the SOD Assay Kit (Sigma-Aldrich) according to the manufacturer's instructions. In brief, 20 μl of each fraction was added to the wells of a 96 well plate followed by 200 μl of the WST Working Solution. Twenty microliters of the Enzyme Working Solution was added to each

well and the plate was incubated for 20 min at 37 °C. The absorbance was read at 450 nm in the SpectraMax 340 microplate reader (Molecular Devices) to calculate the activity. All samples were run in duplicate.

2.9.4. CAT activity—The activities of catalase (CAT) were measured in cytosolic fractions isolated from mouse inner ear tissues using the Catalase Assay Kit (Sigma-Aldrich) according to the manufacturer's instructions. In brief, 25 µl of sample was added to a microcentrifuge tube followed by 50 µl of the 1x Assay Buffer (50 mM potassium phosphate, pH 7.0). The enzymatic reaction was started by adding 25 µl of 200 mM H_2O_2 and the tube was incubated for 5 min at room temperature. The reaction was stopped by adding 900 µl of the Stop Solution. Next, 10 µl out of the enzymatic reaction mixture was transferred to another microcentrifuge tube followed by 990 µl of the Color Reagent. The tube was incubated for 15 min at room temperature and then 200 µl of the colorimetric reaction mixture was transferred to the wells of a 96 well plate. The absorbance was read at 520 nm in the SpectraMax 340 microplate reader (Molecular Devices). The level of CAT activity in each sample was calculated using a standard curve. All samples were run in duplicate.

2.10. Oxidative damage marker

2.10.1. Oxidative DNA damage marker—Levels of the oxidative DNA damage marker, 8-oxoguanine (8-OHdG), were measured using the OxiSelect Oxidative DNA Damage ELISA Kit (Cell Biolabs) according to the manufacturer's instructions. In brief, a 96 well plate was coated with 1 µg/ml 8-OHdG conjugate. Total DNA was isolated from mouse inner ear tissues using the DNeasy Blood & Tissue Kit (Qiagen) according to the manufacturer's instructions. Twelve micrograms per milliliter DNA sample were converted from double-stranded DNA to single-stranded DNA by incubating for 5 min at 95 °C and digested to nucleotides by incubating with 5–20 units of nuclease P1 (Sigma-Aldrich) for 2 h at 37 °C. Nucleotides were then converted to nucleosides by incubating with 5–10 units of alkaline phosphatase (Sigma-Aldrich) for 1 h at 37 °C. The reaction mixture was centrifuged at 6000 × g for 5 min and the supernatant was used for 8-OHdG ELISA. Fifty microliters of the supernatant sample was added to the wells of the 8-OHdG conjugate coated plate and the plate was incubated for 10 min at room temperature. Fifty microliters of the diluted anti-8-OHdG antibody was added to each well and the plate was incubated for 1 h at room temperature. After washing with the 1x Wash Buffer, 100 µl of the diluted horseradish peroxidase-conjugated secondary antibody was added to each well and the plate was incubated for 1 h at room temperature. After washing with the 1x Wash Buffer, the reaction was started by adding 100 µl of the Substrate Solution and the plate was incubated for 10 min at room temperature. The reaction was stopped by adding 100 µl of the Stop Solution. The absorbance was read at 450 nm in the SpectraMax 340 microplate reader (Molecular Devices). The level of 8-OHdG in each sample was calculated using a standard curve. All samples were run in duplicate.

2.10.2. Oxidative protein damage marker—The levels of the oxidative protein damage marker, protein carbonyl, were measured in nuclear, mitochondrial, and cytosolic fractions using the OxyBlot Protein Oxidation Detection Kit (MilliporeSigma) according to

the manufacturer's instructions. In brief, 8 μg of protein in each fraction was added to a microcentrifuge tube, denatured by adding 1 volume of 12% SDS, and derivatized by adding 2 volumes of the 1x DNPH (2,4-dinitrophenylhydrazine) Solution. The tube was incubated for 15 min at room temperature and the reaction was stopped by adding 1.5 volume of the Neutralization Solution. The protein sample was reduced by treatment with 0.74 M 2-mercaptoethanol, fractionated by SDS-PAGE, and transferred to nitrocellulose membranes (Bio-Rad Laboratories). The membranes were incubated with the anti-DNP (2,4-dinitrophenyl) antibody followed by the horseradish peroxidase-conjugated secondary antibody. Chemiluminescent detection reagents (GE Healthcare Life Sciences) were used to visualize proteins. Band intensities were quantified using ImageJ software (National Institutes of Health).

2.11. mtDNA content

Total DNA was isolated from mouse inner ear tissues using the DNeasy Blood & Tissue kit (Qiagen) according to the manufacturer's instructions. Quantitative PCR was performed to determine the copy numbers of mitochondrial DNA (mtDNA) and nuclear DNA (nDNA) as previously described (Evdokimovsky *et al.*, 2011; Picca *et al.*, 2013). The reactions were performed using the iTaq Universal SYBR Green Supermix (Bio-Rad Laboratories) on the Applied Biosystems 7300 Real-Time PCR System (Thermo Fisher Scientific) according to the manufacturer's instructions. The following primers were used:

D-loop forward 5'-AATCTACCATCCTCCGTGAAACC-3';

D-loop reverse 5'-GCCCGGAGCGAGAAGAG-3';

Beta-actin forward 5'-AGCCATGTACGTAGCCATCCA-3';

Beta-actin reverse 5'-TCTCCGGAGTCCATCACAATG-3'.

The D-loop forward and reverse primers targeting the mitochondrial D-loop region were used for the determination of mtDNA copy number, while the beta-actin forward and reverse primers targeting the nuclear beta-actin gene were used for the determination of nDNA copy number (Evdokimovsky *et al.*, 2011). Relative mtDNA content was presented as a ratio of mtDNA to nDNA as previously described (Evdokimovsky *et al.*, 2011; Picca *et al.*, 2013).

2.12. Cell culture analyses

2.12.1. Cell line—House Ear Institute-Organ of Corti 1 (HEI-OC1), a mouse inner ear cell line, was a gift from Dr. Federico Kalinec (Department of Head and Neck Surgery, UCLA). HEI-OC1 cells were cultured in high glucose DMEM containing 10% FBS without antibiotics at 33 °C with 10% CO_2 as previously described (Kalinec *et al.*, 2003).

2.12.2. Txn2 knockdown—HEI-OC1 cells were plated on a 6 well plate (3×10^5 cells per well) and transfected with the siRNA targeted to the *Txn2* gene (OriGene, SR403788) or scrambled control siRNA at 10 nM for 5 d using the Lipofectamine RNAiMAX (Thermo Fisher Scientific) according to the manufacturer's instructions.

2.12.3. Cell lysis—The *Txn2* knockdown HEI-OC1 cells were harvested and lysed with RIPA Buffer (Sigma-Aldrich) and protease inhibitors. The lysate was incubated on ice and then centrifuged at 12000 × g for 10 min at 4 °C to obtain the supernatant (whole cell lysate).

2.12.4. In vitro oxidative stress test and cell viability test—Cell viability tests under oxidative stress were conducted as previously described (Someya *et al.*, 2009; Han *et al.*, 2016b). The *Txn2* knockdown HEI-OC1 cells were replated on a 96 well plate (3×10^4 cells per well) and treated with H_2O_2 at 0, 0.5, 0.75, 1, 1.5, 2, and 2.5 mM for 3 h. After 21 h, H_2O_2 solutions were replaced with medium containing 50 μg/ml neutral red (Sigma-Aldrich) and incubated for 3 h. After washing with PBS, the neutral red solubilizing solution composed of 50% ethanol, 49% water, and 1% glacial acetic acid was added to each well. The absorbance was read at 540 nm in the Synergy HTX microplate reader (BioTek).

2.13. Statistics

Two-way ANOVA (analysis of variance) with Bonferroni's multiple comparisons tests (GraphPad Prism 7) were used to analyze ABR thresholds. One-way ANOVA with Tukey's multiple comparison tests (GraphPad Prism 7) were used to analyze ABR wave I latencies and amplitudes, IHC and OHC losses, and SGN densities. Student's t-tests were used to analyze body weights, Txn2 and TXN1 protein levels, mRNA levels of genes involved in the thioredoxin and glutathione systems and mitochondrial biogenesis, antioxidant enzyme activities, oxidative damage markers, mtDNA contents, and cell viabilities.

3. Results

3.1. Backcrossing Txn2 heterozygous knockout mice onto the CBA/CaJ mouse strain

To investigate the effects of *Txn2* haplodeficiency on cochlear antioxidant defenses and age-related cochlear pathology and hearing loss, $Txn2^{+/-}$ mice were backcrossed for four generations onto the CBA/CaJ mouse strain, a well-established model of late onset AHL (Zheng *et al.*, 1999; Noben-Trauth *et al.*, 2003; Ohlemiller, 2006; Han and Someya, 2013). We genotyped N4 wild-type (CBA/CaJ-WT or WT) and heterozygous (CBA/CaJ-$Txn2^{+/-}$ or $Txn2^{+/-}$) mice by *Txn2* PCR (Fig. 1A) and *Cdh23* sequencing (Fig. 1B). We confirmed that all WT and $Txn2^{+/-}$ mice had the same wild-type *Cdh23* genotype ($Cdh23^{753G/753G}$) (Fig. 1B). $Txn2^{+/-}$ mice in the CBA/CaJ background appeared phenotypically normal. No differences in body weights were observed between male or female WT and $Txn2^{+/-}$ mice from 4 months of age until 24 months of age (Fig. 1C–D).

3.2. Localization of TXN2 protein in mouse cochlea

To confirm that TXN2 protein is expressed in mouse inner ears and to validate the PCR genotyping results, we measured the levels of TXN2 protein in the nuclei, mitochondria, and cytosol of the inner ear tissues from 7–8 months old WT and $Txn2^{+/-}$ mice by Western blot. We confirmed that TXN2 protein was detected in the mitochondria, whereas no or little TXN2 protein was detected in the nuclei or cytosol (Fig. 2A, left panel). $Txn2^{+/-}$ mice displayed a 58% decrease in TXN2 protein levels in the mitochondria of the inner ears compared to WT mice (Fig. 2A, right panel). Next, we investigated the localization of TXN2

protein in the cochlear tissues from 3–5 months old WT and *Txn2*$^{+/-}$ mice by confocal-based immunohistochemistry. TXN2 immunostaining was evident in numerous cell types of the WT mouse cochlea (Fig. 2B–M). Cells of the organ of Corti (OC) including hair cells (HCs) and supporting cells (SCs), spiral ganglion neurons (SGNs), and cells of the stria vascularis (SV) showed varying levels of TXN2 immunostaining (Fig. 2B–M). High magnification of the SGNs showed a clear punctate pattern, consistent with the expected mitochondrial localization of TXN2 protein (Fig. 2H–J). The heterozygous *Txn2*$^{+/-}$ mouse cochlea showed detectable TXN2 immunostaining similar to the WT mouse cochlea, but the intensity was markedly reduced as illustrated by images from the OC (Fig. 2N–P).

3.3. Txn2 haplodeficiency does not affect auditory function in young, middle-aged, or old mice

To investigate the effects of *Txn2* haplodeficiency on auditory function under normal physiological conditions or across the lifespan, we measured auditory brainstem response (ABR) thresholds with a tone burst stimulus at 4, 8, 16, 32, 48, and 64 kHz in male and female WT and *Txn2*$^{+/-}$ mice at 3–5, 15–16, and 23–25 months of age. At 3–5 months of age (young mice), there were no differences in ABR thresholds at all the frequencies measured between male or female WT and *Txn2*$^{+/-}$ mice (Fig. 3A–B). At 23–25 months of age (old mice), both WT and *Txn2*$^{+/-}$ mice displayed age-related increases in ABR thresholds (Fig. 3A–B), consistent with the previous report that the CBA/CaJ mouse strain exhibits late onset AHL beginning at 17–20 months of age (Zheng *et al.*, 1999; Ohlemiller, 2006; Han and Someya, 2013). However, there were no differences in ABR thresholds at all the frequencies measured between WT and *Txn2*$^{+/-}$ mice, male or female, at 15–16 (middle-aged mice) or 23–25 months of age (Fig. 3A–B). In mice, ABRs typically consist of five positive waves; wave I represents activity from the auditory nerve and waves II-V represent neural transmission within the central auditory system (Zhou *et al.*, 2006). The ABR wave I reflects the synchronized firing of spiral ganglion neurons (SGNs) at sound onset, triggered by the synaptic output from cochlear inner hair cells (IHCs) (Becker *et al.*, 2018). In mice, loss of synapses or cochlear nerve terminals innervating IHCs is also associated with a decrease in the suprathreshold amplitude of ABR wave I (Kujawa and Liberman, 2009; Furman *et al.*, 2013; Hickox and Liberman, 2014; Liberman *et al.*, 2015; Mehraei *et al.*, 2016) and ABR wave-IV latency shift (Mehraei et al 2016). To further assess hearing sensitivity and functional integrity of the auditory nerve, we measured latencies and amplitudes for ABR wave I with a click stimulus of 100 dB peak SPL in male and female WT and *Txn2*$^{+/-}$ mice at 3–5, 15–16, and 23–25 months of age. In agreement with the ABR threshold results, there were no differences in ABR wave I latencies or amplitudes between WT and *Txn2*$^{+/-}$ mice, male or female, at 3–5, 15–16, or 23–25 months of age (Fig. 3C–F). Together, these physiological results indicate that *Txn2* haplodeficiency does not affect auditory function in mice across the lifespan.

3.4. Txn2 haplodeficiency does not cause degeneration of cochlear hair cells and SGNs in young mice or accelerate age-related degeneration of cochlear hair cells and SGNs in old mice

The major sites of cochlear pathology typically include sensory hair cells, spiral ganglion neurons (SGNs), and/or stria vascularis (Gates and Mills, 2005; Yamasoba *et al.*, 2013). To

validate the physiological results and to investigate the effects of *Txn2* haplodeficiency on age-related cochlear hair cell loss, we prepared cochleograms from male and female WT and *Txn2*$^{+/-}$ mice at 3–5 and 23–25 months of age. At 3–5 months of age, there were no or little loss of inner hair cells (IHCs) or outer hair cells (OHCs) in the apical, middle, or basal cochlear regions in male or female WT or *Txn2*$^{+/-}$ mice (Fig. 4A–B). At 23–25 months of age, a slight increase in OHC losses in the apical cochlear region was observed in male *Txn2*$^{+/-}$ mice compared to age-matched WT mice, but overall, there were no or little loss of IHCs or OHCs in the apical, middle, or basal cochlear regions in male or female WT or *Txn2*$^{+/-}$ mice (Fig. 4A–B). To investigate whether *Txn2* haplodeficiency affects age-related SGN degeneration, we counted SGNs in the basal region of male and female WT and *Txn2*$^{+/-}$ mice at 3–5 and 23–25 months of age. At 3–5 months of age, there were no differences in SGN densities in the basal cochlear region between WT and *Txn2*$^{+/-}$ mice, male or female (Fig. 5A–B). At 23–25 months of age, there were also no differences in SGN densities in the basal cochlear region between WT and *Txn2*$^{+/-}$ mice, male or female (Fig. 5A–B). Together, these histological results validate the physiological test results and indicate that *Txn2* haplodeficiency does not cause degeneration of cochlear hair cells or SGNs in young mice or accelerate age-related degeneration of cochlear hair cells or SGNs in old mice.

3.5. Txn2 haplodeficiency does not affect antioxidant defenses, oxidative damage, or mitochondrial biogenesis in mouse inner ears

The thioredoxin and glutathione systems are thought to be the two major antioxidant defense systems in mammalian cells (Lu and Holmgren, 2014; Ribas *et al.*, 2014). To investigate the effects of *Txn2* haplodeficiency on antioxidant defenses in mouse inner ears, we measured mRNA levels of genes involved in the thioredoxin (*Txn1*, *Txn2*, *Txnrd1*, *Txnrd2*, *Prdx2*, *Prdx3*) and glutathione (*Gsr*, *Gpx1*, *Gss*, *Gclc*, and *Gclm*) systems in the inner ear tissues from 3–5 months old WT and *Txn2*$^{+/-}$ mice. Because there were no sex differences in auditory functions or cochlear pathologies in WT and *Txn2*$^{+/-}$ mice, subsequent cochlear tissue analysis was conducted in either male or female mice. As expected, *Txn2*$^{+/-}$ mice displayed a 54% decrease in *Txn2* mRNA levels in the inner ears compared to WT mice (Fig. 6A). However, there were no differences in mRNA levels of *Txn1*, *Txnrd1*, *Txnrd2*, *Prdx2*, *Prdx3*, *Gsr*, *Gpx1*, *Gss*, *Gclc*, or *Gclm* in the inner ears between WT and *Txn2*$^{+/-}$ mice (Fig. 6A–B). We also measured the activities of TXNRD, GPX, SOD, and CAT in the nuclei, mitochondria, or cytosol of the inner ear tissues from 3–5 months old WT and *Txn2*$^{+/-}$ mice. There were no differences in the activities of TXNRD, GPX, SOD, or CAT in the nuclei, mitochondria, or cytosol of the inner ears between WT and *Txn2*$^{+/-}$ mice (Fig. 6C–F). Furthermore, we measured TXN1 protein levels in the cytosol of the inner ear tissues from 3–5 months old WT and *Txn2*$^{+/-}$ mice. There were no differences in TXN1 protein levels in the cytosol of the inner ears between WT and *Txn2*$^{+/-}$ mice (Fig. 6G), supporting the *Txn1* mRNA expression analysis results observed in Fig. 6A. If TXN2 plays an essential role in protecting inner ear cells against oxidative stress, *Txn2* haplodeficiency may result in increased oxidative damage in the inner ears. To test this hypothesis, we measured the levels of 8-oxoguanine (8-OHdG), a marker of oxidative DNA damage, in the inner ear tissues from 3–5 months old WT and *Txn2*$^{+/-}$ mice. There were no differences in 8-OHdG levels in the inner ears between WT and *Txn2*$^{+/-}$ mice (Fig. 6H). Next, we measured the levels of

protein carbonyl, a marker of oxidative protein damage, in the nuclei, mitochondria, and cytosol of the inner ear tissues from 3–5 months old WT and *Txn2*$^{+/-}$ mice. There were no differences in protein carbonyl levels in the nuclei, mitochondria, or cytosol of the inner ears between WT and *Txn2*$^{+/-}$ mice (Fig. 6I). To further investigate whether *Txn2* haplodeficiency affects cell viability under oxidative stress conditions, we conducted *in vitro* oxidative stress tests using H_2O_2 followed by cell viability tests in controls and *Txn2* knockdown HEI-OC1 cells. siRNA-mediated knockdown of *Txn2* resulted in a 67% decrease in TXN2 protein levels in HEI-OC1 cells (Fig. 7A). In agreement with the inner ear tissue analysis results, there were no differences in cell viabilities at various H_2O_2 concentrations between controls and *Txn2* knockdown HEI-OC1 cells (Fig. 7B). Lastly, to investigate the effects of *Txn2* haplodeficiency on mitochondrial biogenesis in mouse inner ears, we measured mRNA levels of genes involved in mitochondrial biogenesis (*Tfam*, *Ppargc1a*, and *Nrf1*) in the inner ear tissues from 3–5 months old WT and *Txn2*$^{+/-}$ mice. There were no differences in mRNA levels of *Tfam*, *Ppargc1a*, or *Nrf1* in the inner ears between WT and *Txn2*$^{+/-}$ mice (Fig. 8A). We also measured mitochondrial DNA (mtDNA) contents in the inner ear tissues from 3–5 months old WT and *Txn2*$^{+/-}$ mice. There were no differences in mtDNA contents in the inner ears between WT and *Txn2*$^{+/-}$ mice (Fig. 8B). Together, these molecular and biochemical analysis results suggest that *Txn2* haplodeficiency does not affect the thioredoxin or glutathione antioxidant defense, mitochondrial or cytosolic antioxidant defense, oxidative damage, or mitochondrial biogenesis in mouse inner ears under normal physiological conditions or cell viability under oxidative stress conditions in mouse inner ear cells.

4. Discussion

In the current study, we have demonstrated that TXN2 protein is detected and localized in hair cells, SGNs, and SV regions of the mouse cochlea. We found that *Txn2*$^{+/-}$ mice displayed decreased TXN2 protein levels in the mitochondria of the inner ears compared to WT mice. However, *Txn2* haplodeficiency did not affect the thioredoxin or glutathione antioxidant defenses in both the mitochondria and cytosol of the inner ears of young mice. There were no differences in the levels of mitochondrial biogenesis markers, mtDNA contents, or oxidative DNA and protein damage markers in the inner ears between young WT and *Txn2*$^{+/-}$ mice. In a mouse inner ear cell line, knockdown of *Txn2* did not affect cell viability under H_2O_2 treatment. Consistent with the tissue and cell line analysis results, there were no differences in hair cell losses or SGN densities between young or old WT and *Txn2*$^{+/-}$ mice. Furthermore, *Txn2* haplodeficiency did not affect ABR threshold, wave I latency, or wave I amplitude in young, middle-aged, or old mice. Consistent with our findings, previous studies have demonstrated that *Txn2* haplodeficiency or *Txn2* overexpression does not affect the protein levels or activities of several antioxidant enzymes and antioxidants (Nonn *et al.*, 2003; Perez *et al.*, 2008; He *et al.*, 2008): Although heterozygous *Txn2*$^{+/-}$ mice displayed decreased TXN2 protein levels in the mitochondria of the liver, skeletal muscle, heart, and brain compared to WT mice (Nonn *et al.*, 2003; Perez *et al.*, 2008), the protein levels of antioxidant enzymes, including SOD2, CAT, and PRDX3, remained unchanged in the liver mitochondria between WT and *Txn2*$^{+/-}$ mice (Nonn *et al.*, 2003). There were also no differences in the activities of antioxidant enzymes, including

SOD1, SOD2, CAT, GPX, PRDX3, and TXN1, or the levels of total glutathione in the liver between WT and *Txn2*$^{+/-}$ mice (Perez *et al.*, 2008). Furthermore, although *Txn2*-overexpressing transgenic (Tg) mice displayed increased TXN2 activities in the liver mitochondria compared to WT mice, there were no differences in TXNRD2 activities, TXN2 redox potentials, mitochondrial membrane potentials, or cytochrome c contents in the mitochondria of the liver between WT and *Txn2* Tg mice (He *et al.*, 2008). In line with these reports, *Txn2* knockdown did not induce cytotoxicity or alter mitochondrial biosynthesis or the protein levels of electron transport chain components in neonatal rat ventricular cardiomyocytes (Hu *et al.*, 2018). Therefore, our findings and the previous reports suggest that *Txn2* haplodeficiency does not affect cochlear antioxidant defenses, accelerate degeneration of cochlear hair cells or SGNs, or affect auditory function in mice across the lifespan.

The balance between antioxidant defenses and oxidants is thought to be determined by the ratios of interconvertible forms of redox couples such as reduced glutathione/oxidized glutathione (GSH/GSSG), reduced TXN/oxidized TXN, NADH/NAD^+, and NADPH/$NADP^+$ in mammalian cells (Rebrin and Sohal, 2008; White *et al.*, 2018). However, a previous study has shown that *Txn2* haplodeficiency does not affect GPX, SOD1, SOD2, CAT, or TXN1 activities or the levels of total glutathione in the liver between WT and *Txn2*$^{+/-}$ mice (Perez *et al.*, 2008). In agreement with this report, we found that there were no differences in mRNA levels of genes involved in the glutathione antioxidant defense system, including *Gsr*, *Gpx1*, *Gss*, *Gclc*, or *Gclm,* in the inner ears between WT and *Txn2*$^{+/-}$ mice (Fig. 6B). There were also no differences in GPX activities in the nuclei, mitochondria, or cytosol of the inner ears between WT and *Txn2*$^{+/-}$ mice (Fig. 6D). Therefore, we speculate that a partial loss of TXN2 does not affect the glutathione antioxidant defense system in the cochlea under normal physiological conditions.

Acknowledgements

This research was supported by R03 DC011840, R01 DC012552, R01 DC014437, P30 AG028740 from the National Institute of Health (National Institute on Deafness and Communication Disorders and National Institute on Aging) and the Claude D. Pepper Older Americans Independence Centers at the University of Florida, American Cancer Society (131062-RSG-17-171-01-DMC), and the Japan Society for the Promotion of Science (JSPS) Grant-in-Aid for Scientific Research (A) (Grant number, 26253081) and for Scientific Research (S) (Grant number, 23228003).

References

Arner ES & Holmgren A (2000). Physiological functions of thioredoxin and thioredoxin reductase. Eur J Biochem 267(20): 6102–6109. [PubMed: 11012661]

Balaban RS, Nemoto S & Finkel T (2005). Mitochondria, oxidants, and aging. Cell 120(4): 483–495. [PubMed: 15734681]

Becker L, Schnee ME, Niwa M, Sun W, Maxeiner S, Talaei S, Kachar B, Rutherford MA & Ricci AJ (2018). The presynaptic ribbon maintains vesicle populations at the hair cell afferent fiber synapse. Elife 7.

Bertini R, Howard OM, Dong HF, Oppenheim JJ, Bizzarri C, Sergi R, Caselli G, Pagliei S, Romines B, Wilshire JA, Mengozzi M, Nakamura H, Yodoi J, Pekkari K, Gurunath R, Holmgren A, Herzenberg LA, Herzenberg LA & Ghezzi P (1999). Thioredoxin, a redox enzyme released in infection and inflammation, is a unique chemoattractant for neutrophils, monocytes, and T cells. J Exp Med 189(11): 1783–1789. [PubMed: 10359582]

Birben E, Sahiner UM, Sackesen C, Erzurum S & Kalayci O (2012). Oxidative stress and antioxidant defense. World Allergy Organ J 5(1): 9–19. [PubMed: 23268465]

Chae HZ, Kang SW & Rhee SG (1999). Isoforms of mammalian peroxiredoxin that reduce peroxides in presence of thioredoxin. Methods Enzymol 300: 219–226. [PubMed: 9919524]

Chen Y, Cai J, Murphy TJ & Jones DP (2002). Overexpressed human mitochondrial thioredoxin confers resistance to oxidant-induced apoptosis in human osteosarcoma cells. J Biol Chem 277(36): 33242–33248. [PubMed: 12032145]

Cui H, Kong Y & Zhang H (2012). Oxidative stress, mitochondrial dysfunction, and aging. J Signal Transduct 2012: 646354. [PubMed: 21977319]

Damdimopoulos AE, Miranda-Vizuete A, Pelto-Huikko M, Gustafsson JA & Spyrou G (2002). Human mitochondrial thioredoxin. Involvement in mitochondrial membrane potential and cell death. J Biol Chem 277(36): 33249–33257. [PubMed: 12080052]

Ding D, Jiang H, Chen GD, Longo-Guess C, Muthaiah VP, Tian C, Sheppard A, Salvi R & Johnson KR (2016). N-acetyl-cysteine prevents age-related hearing loss and the progressive loss of inner hair cells in gamma-glutamyl transferase 1 deficient mice. Aging (Albany NY) 8(4): 730–750. [PubMed: 26977590]

Ding D, Qi W, Yu D, Jiang H, Han C, Kim MJ, Katsuno K, Hsieh YH, Miyakawa T, Salvi R, Tanokura M & Someya S (2013). Addition of exogenous NAD+ prevents mefloquine-induced neuroaxonal and hair cell degeneration through reduction of caspase-3-mediated apoptosis in cochlear organotypic cultures. PLoS One 8(11): e79817. [PubMed: 24223197]

Evans P & Halliwell B (1999). Free radicals and hearing. Cause, consequence, and criteria. Ann N Y Acad Sci 884: 19–40. [PubMed: 10842581]

Evdokimovsky EV, Ushakova TE, Kudriavtcev AA & Gaziev AI (2011). Alteration of mtDNA copy number, mitochondrial gene expression and extracellular DNA content in mice after irradiation at lethal dose. Radiat Environ Biophys 50(1): 181–188. [PubMed: 20814800]

Furman AC, Kujawa SG & Liberman MC (2013). Noise-induced cochlear neuropathy is selective for fibers with low spontaneous rates. J Neurophysiol 110(3): 577–586. [PubMed: 23596328]

Gates GA & Mills JH (2005). Presbycusis. Lancet 366(9491): 1111–1120. [PubMed: 16182900]

Han C, Kim MJ, Ding D, Park HJ, White K, Walker L, Gu T, Tanokura M, Yamasoba T, Linser P, Salvi R & Someya S (2017). GSR is not essential for the maintenance of antioxidant defenses in mouse cochlea: Possible role of the thioredoxin system as a functional backup for GSR. PLoS One 12(7): e0180817. [PubMed: 28686716]

Han C, Linser P, Park HJ, Kim MJ, White K, Vann JM, Ding D, Prolla TA & Someya S (2016). Sirt1 deficiency protects cochlear cells and delays the early onset of age-related hearing loss in C57BL/6 mice. Neurobiol Aging 43: 58–71. [PubMed: 27255815]

Han C & Someya S (2013). Mouse models of age-related mitochondrial neurosensory hearing loss. Mol Cell Neurosci 55: 95–100. [PubMed: 22820179]

He M, Cai J, Go YM, Johnson JM, Martin WD, Hansen JM & Jones DP (2008). Identification of thioredoxin-2 as a regulator of the mitochondrial permeability transition. Toxicol Sci 105(1): 44–50. [PubMed: 18550601]

Hickox AE & Liberman MC (2014). Is noise-induced cochlear neuropathy key to the generation of hyperacusis or tinnitus? J Neurophysiol 111(3): 552–564. [PubMed: 24198321]

Hirota K, Murata M, Sachi Y, Nakamura H, Takeuchi J, Mori K & Yodoi J (1999). Distinct roles of thioredoxin in the cytoplasm and in the nucleus. A two-step mechanism of redox regulation of transcription factor NF-kappaB. J Biol Chem 274(39): 27891–27897. [PubMed: 10488136]

Holmgren A (1985). Thioredoxin. Annu Rev Biochem 54: 237–271. [PubMed: 3896121]

Holmgren A (1989). Thioredoxin and glutaredoxin systems. J Biol Chem 264(24): 13963–13966. https://www.jax.org/strain/000654 https://www.taconic.com/knockout-mouse/txn2-trapped. [PubMed: 2668278]

Hu C, Zhang H, Qiao Z, Wang Y, Zhang P & Yang D (2018). Loss of thioredoxin 2 alters mitochondrial respiratory function and induces cardiomyocyte hypertrophy. Exp Cell Res 372(1): 61–72. [PubMed: 30236513]

Jiang H, Talaska AE, Schacht J & Sha SH (2007). Oxidative imbalance in the aging inner ear. Neurobiol Aging 28(10): 1605–1612. [PubMed: 16920227]

Kalinec GM, Webster P, Lim DJ & Kalinec F (2003). A cochlear cell line as an in vitro system for drug ototoxicity screening. Audiol Neurootol 8(4): 177–189. [PubMed: 12811000]

Kang SW, Chae HZ, Seo MS, Kim K, Baines IC & Rhee SG (1998). Mammalian peroxiredoxin isoforms can reduce hydrogen peroxide generated in response to growth factors and tumor necrosis factor-alpha. J Biol Chem 273(11): 6297–6302. [PubMed: 9497357]

Kim MJ, Haroon S, Chen GD, Ding D, Wanagat J, Liu L, Zhang Y, White K, Park HJ, Han C, Boyd K, Caicedo I, Evans K, Linser PJ, Tanokura M, Prolla T, Salvi R, Vermulst M & Someya S (2019). Increased burden of mitochondrial DNA deletions and point mutations in early-onset age-related hearing loss in mitochondrial mutator mice. Exp Gerontol 125: 110675. [PubMed: 31344454]

Kokotas H, Petersen MB & Willems PJ (2007). Mitochondrial deafness. Clin Genet 71(5): 379–391. [PubMed: 17489842]

Kujawa SG & Liberman MC (2009). Adding insult to injury: cochlear nerve degeneration after “temporary” noise-induced hearing loss. J Neurosci 29(45): 14077–14085. [PubMed: 19906956]

Liberman LD, Suzuki J & Liberman MC (2015). Dynamics of cochlear synaptopathy after acoustic overexposure. J Assoc Res Otolaryngol 16(2): 205–219. [PubMed: 25676132]

Lillig CH & Holmgren A (2007). Thioredoxin and related molecules--from biology to health and disease. Antioxid Redox Signal 9(1): 25–47. [PubMed: 17115886]

Lin MT & Beal MF (2006). Mitochondrial dysfunction and oxidative stress in neurodegenerative diseases. Nature 443(7113): 787–795. [PubMed: 17051205]

Lu J & Holmgren A (2014). The thioredoxin antioxidant system. Free Radic Biol Med 66: 75–87. [PubMed: 23899494]

McFadden SL, Ding D, Reaume AG, Flood DG & Salvi RJ (1999). Age-related cochlear hair cell loss is enhanced in mice lacking copper/zinc superoxide dismutase. Neurobiol Aging 20(1): 1–8. [PubMed: 10466888]

Mehraei G, Hickox AE, Bharadwaj HM, Goldberg H, Verhulst S, Liberman MC & Shinn-Cunningham BG (2016). Auditory Brainstem Response Latency in Noise as a Marker of Cochlear Synaptopathy. J Neurosci 36(13): 3755–3764. [PubMed: 27030760]

Muller M, von Hunerbein K, Hoidis S & Smolders JW (2005). A physiological place-frequency map of the cochlea in the CBA/J mouse. Hear Res 202(1–2): 63–73. [PubMed: 15811700]

Nakamura H, Nakamura K & Yodoi J (1997). Redox regulation of cellular activation. Annu Rev Immunol 15: 351–369. [PubMed: 9143692]

Noben-Trauth K, Zheng QY & Johnson KR (2003). Association of cadherin 23 with polygenic inheritance and genetic modification of sensorineural hearing loss. Nat Genet 35(1): 21–23.

Nonn L, Williams RR, Erickson RP & Powis G (2003). The absence of mitochondrial thioredoxin 2 causes massive apoptosis, exencephaly, and early embryonic lethality in homozygous mice. Mol Cell Biol 23(3): 916–922. [PubMed: 12529397]

Ohlemiller KK (2006). Contributions of mouse models to understanding of age- and noise-related hearing loss. Brain Res 1091(1): 89–102. [PubMed: 16631134]

Park HJ, Kim MJ, Rothenberger C, Kumar A, Sampson EM, Ding D, Han C, White K, Boyd K, Manohar S, Kim YH, Ticsa MS, Gomez AS, Caicedo I, Bose U, Linser PJ, Miyakawa T, Tanokura M, Foster TC, Salvi R & Someya S (2019). GSTA4 mediates reduction of cisplatin ototoxicity in female mice. Nat Commun 10(1): 4150. [PubMed: 31515474]

Perez VI, Lew CM, Cortez LA, Webb CR, Rodriguez M, Liu Y, Qi W, Li Y, Chaudhuri A, Van Remmen H, Richardson A & Ikeno Y (2008). Thioredoxin 2 haploinsufficiency in mice results in impaired mitochondrial function and increased oxidative stress. Free Radic Biol Med 44(5): 882–892. [PubMed: 18164269]

Picca A, Fracasso F, Pesce V, Cantatore P, Joseph AM, Leeuwenburgh C, Gadaleta MN & Lezza AM (2013). Age- and calorie restriction-related changes in rat brain mitochondrial DNA and TFAM binding. Age (Dordr) 35(5): 1607–1620. [PubMed: 22945739]

Powis G & Montfort WR (2001). Properties and biological activities of thioredoxins. Annu Rev Pharmacol Toxicol 41: 261–295. [PubMed: 11264458]

Rebrin I & Sohal RS (2008). Pro-oxidant shift in glutathione redox state during aging. Adv Drug Deliv Rev 60(13–14): 1545–1552. [PubMed: 18652861]

Ribas V, Garcia-Ruiz C & Fernandez-Checa JC (2014). Glutathione and mitochondria. Front Pharmacol 5: 151. [PubMed: 25024695]

Saitoh M, Nishitoh H, Fujii M, Takeda K, Tobiume K, Sawada Y, Kawabata M, Miyazono K & Ichijo H (1998). Mammalian thioredoxin is a direct inhibitor of apoptosis signal-regulating kinase (ASK) 1. EMBO J 17(9): 2596–2606. [PubMed: 9564042]

Schenk H, Klein M, Erdbrugger W, Droge W & Schulze-Osthoff K (1994). Distinct effects of thioredoxin and antioxidants on the activation of transcription factors NF-kappa B and AP-1. Proc Natl Acad Sci U S A 91(5): 1672–1676. [PubMed: 8127864]

Schriner SE, Linford NJ, Martin GM, Treuting P, Ogburn CE, Emond M, Coskun PE, Ladiges W, Wolf N, Van Remmen H, Wallace DC & Rabinovitch PS (2005). Extension of murine life span by overexpression of catalase targeted to mitochondria. Science 308(5730): 1909–1911. [PubMed: 15879174]

Silberstein DS, McDonough S, Minkoff MS & Balcewicz-Sablinska MK (1993). Human eosinophil cytotoxicity-enhancing factor. Eosinophil-stimulating and dithiol reductase activities of biosynthetic (recombinant) species with COOH-terminal deletions. J Biol Chem 268(12): 9138–9142. [PubMed: 8473353]

Someya S & Prolla TA (2010). Mitochondrial oxidative damage and apoptosis in age-related hearing loss. Mech Ageing Dev 131(7–8): 480–486. [PubMed: 20434479]

Someya S, Xu J, Kondo K, Ding D, Salvi RJ, Yamasoba T, Rabinovitch PS, Weindruch R, Leeuwenburgh C, Tanokura M & Prolla TA (2009). Age-related hearing loss in C57BL/6J mice is mediated by Bak-dependent mitochondrial apoptosis. Proc Natl Acad Sci U S A 106(46): 19432–19437. [PubMed: 19901338]

Svensson MJ & Larsson J (2007). Thioredoxin-2 affects lifespan and oxidative stress in Drosophila. Hereditas 144(1): 25–32. [PubMed: 17567437]

Tanaka T, Hosoi F, Yamaguchi-Iwai Y, Nakamura H, Masutani H, Ueda S, Nishiyama A, Takeda S, Wada H, Spyrou G & Yodoi J (2002). Thioredoxin-2 (TRX-2) is an essential gene regulating mitochondria-dependent apoptosis. EMBO J 21(7): 1695–1703. [PubMed: 11927553]

White K, Kim MJ, Ding D, Han C, Park HJ, Meneses Z, Tanokura M, Linser P, Salvi R & Someya S (2017). G6pd Deficiency Does Not Affect the Cytosolic Glutathione or Thioredoxin Antioxidant Defense in Mouse Cochlea. J Neurosci 37(23): 5770–5781. [PubMed: 28473643]

White K, Kim MJ, Han C, Park HJ, Ding D, Boyd K, Walker L, Linser P, Meneses Z, Slade C, Hirst J, Santostefano K, Terada N, Miyakawa T, Tanokura M, Salvi R & Someya S (2018). Loss of IDH2 Accelerates Age-related Hearing Loss in Male Mice. Sci Rep 8(1): 5039. [PubMed: 29567975]

Yamasoba T, Lin FR, Someya S, Kashio A, Sakamoto T & Kondo K (2013). Current concepts in age-related hearing loss: epidemiology and mechanistic pathways. Hear Res 303: 30–38. [PubMed: 23422312]

Zhang P, Liu B, Kang SW, Seo MS, Rhee SG & Obeid LM (1997). Thioredoxin peroxidase is a novel inhibitor of apoptosis with a mechanism distinct from that of Bcl-2. J Biol Chem 272(49): 30615–30618. [PubMed: 9388194]

Zheng QY, Johnson KR & Erway LC (1999). Assessment of hearing in 80 inbred strains of mice by ABR threshold analyses. Hear Res 130(1–2): 94–107. [PubMed: 10320101]

Zhou X, Jen PH, Seburn KL, Frankel WN & Zheng QY (2006). Auditory brainstem responses in 10 inbred strains of mice. Brain Res 1091(1): 16–26. [PubMed: 16516865]

Highlights

- *Txn2* haplodeficiency result in decreased TXN2 protein levels in mouse inner ears
- *Txn2* haplodeficiency does not affect inner ear antioxidant defenses in mice
- *Txn2* haplodeficiency does not accelerate degeneration of cochlear cells in mice
- *Txn2* haplodeficiency does not accelerate age-related hearing loss in mice

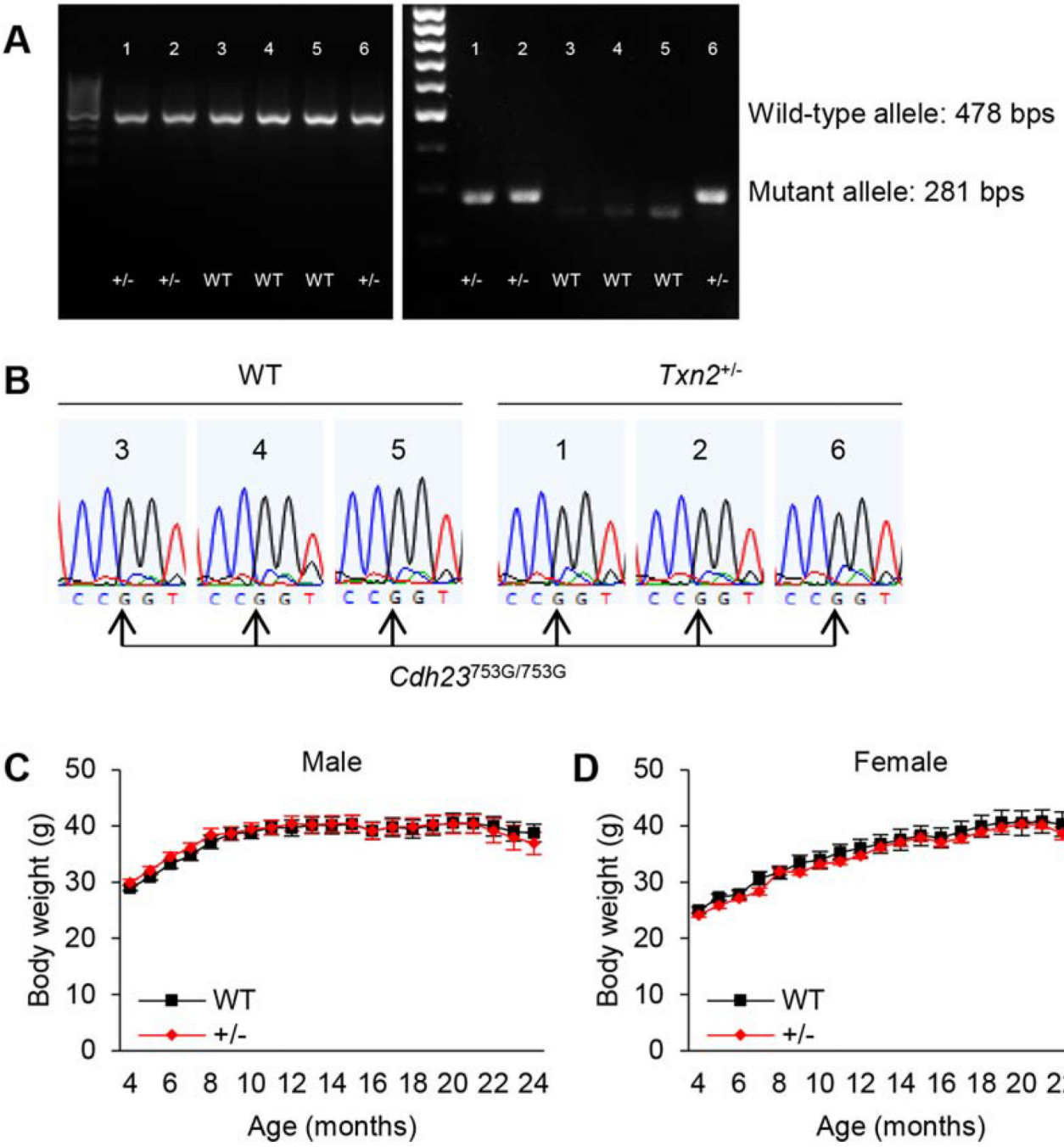

Fig. 1.

Genotyping and body weight of WTand *Txn2* $^{+/-}$ mice. (A) *Txn2* genotyping: PCR products were separated on a 2% agarose gel. The expected band sizes for the wild-type and mutant alleles were 478 and 281 bps, respectively. (B) *Cdh23* genotyping: The *Cdh23* gene in WT and *Txn2*$^{+/-}$ mice was sequenced ($N = 3$). All the mice examined had the same wild-type *Cdh23* genotype (*Cdh23*$^{753G/753G}$). C-D: The body weight of male (C) and female (D) WT and *Txn2*$^{+/-}$ mice was measured every month from 4 months of age until 24 months of age ($N = 7–12$). Data are shown as means ± SEM.

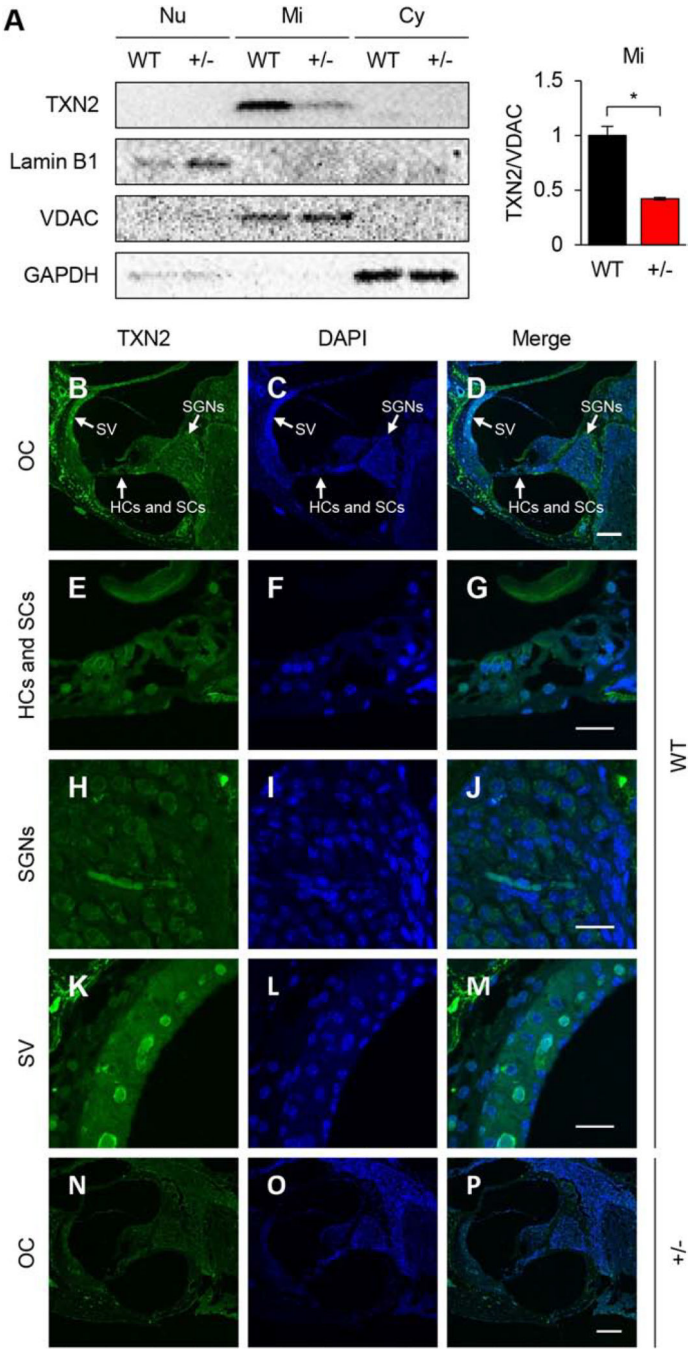

Fig. 2.

Localization of TXN2 protein in mouse cochlea. (A) Western blot of TXN2 protein levels was performed in the nuclei (Nu), mitochondria (Mi), and cytosol (Cy) of the inner ear tissues from 7–8 months old WT and *Txn2*$^{+/-}$ mice ($N = 3$). Lamin B1, VDAC, and GAPDH were used as nuclear, mitochondrial, and cytosolic loading controls, respectively. Data are shown as means ± SEM. *$p < 0.05$, WT vs. +/−. B-P: TXN2 staining (green; B, E, H, K, N), DAPI staining (nuclear marker; blue; C, F, I, L, O), and merged staining (D, G, J, M, P) were detected in the organ of Corti (OC) regions (B-D, N-P), hair cells (HCs) and

supporting cells (SCs) (E-G), spiral ganglion neurons (SGNs) (H-J), and stria vascularis (SV) (K-M) of the cochlear tissues from 3–5 months old WT (B-M) and *Txn2*$^{+/-}$ (N-P) mice ($N = 5$). Scale bar = 100 μm (D, P), 20 μm (G, J, M).

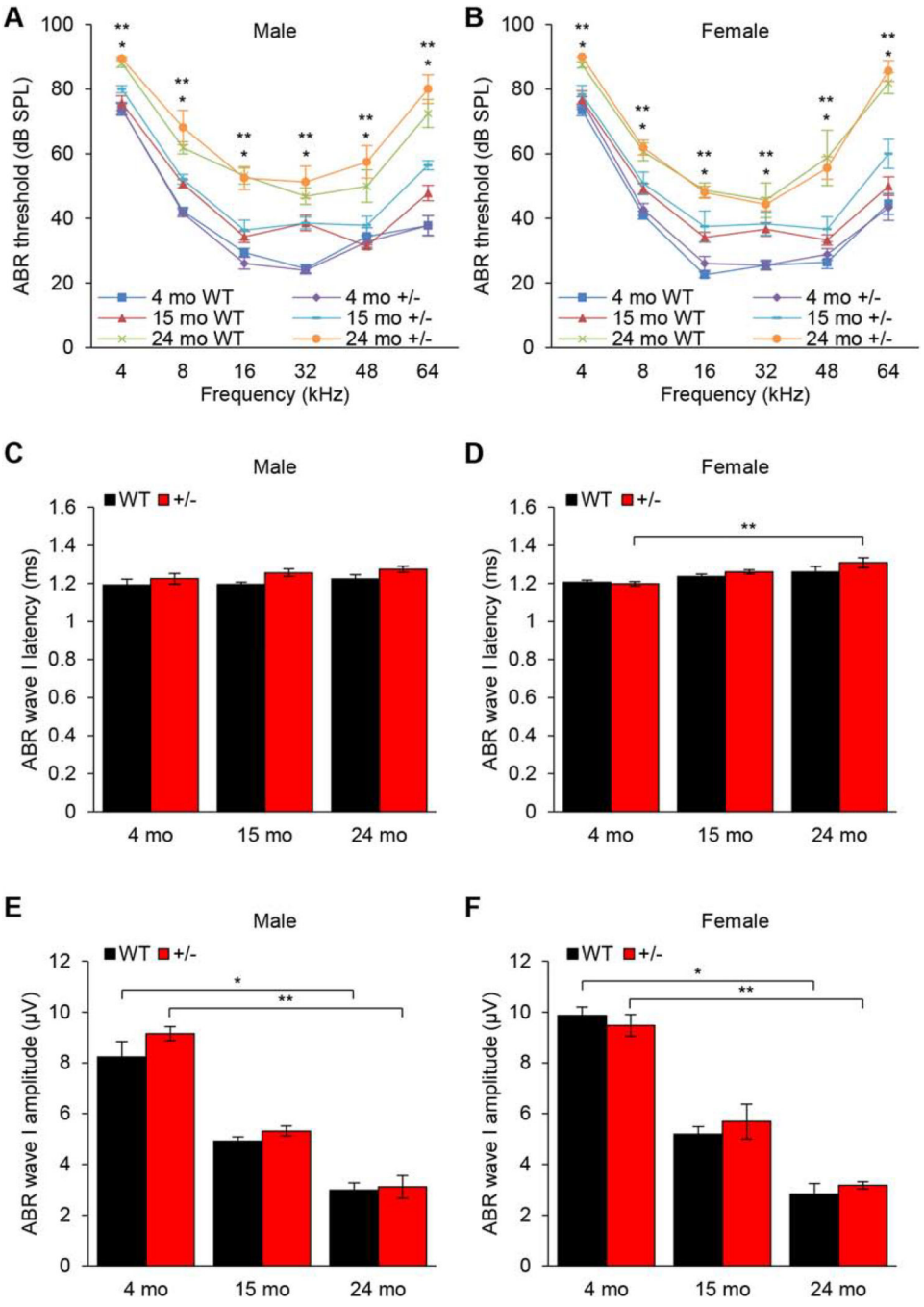

Fig. 3.

Effects of *Txn2* haplodeficiency on auditory function in mice across the lifespan. A-B: ABR thresholds were measured with a tone burst stimulus at 4, 8, 16, 32, 48, and 64 kHz in male (A) and female (B) WT and $Txn2^{+/-}$ mice at 3–5 (4), 15–16 (15), and 23–25 (24) months of age (N = 6–10). C-D: Latencies for ABR wave I were measured with a click stimulus of 100 dB SPL in male (C) and female (D) WT and $Txn2^{+/-}$ mice at 4, 15, and 24 months of age (N = 6–10). E-F: Amplitudes for ABR wave I were measured with a click stimulus of 100 dB SPL in male (E) and female (F) WT and $Txn2^{+/-}$ mice at 4, 15, and 24 months of age (N =

6–10). Data are shown as means ± SEM. *$p < 0.05$, 4 mo WT vs. 24 mo WT, **$p < 0.05$, 4 mo +/− vs. 24 mo +/−.

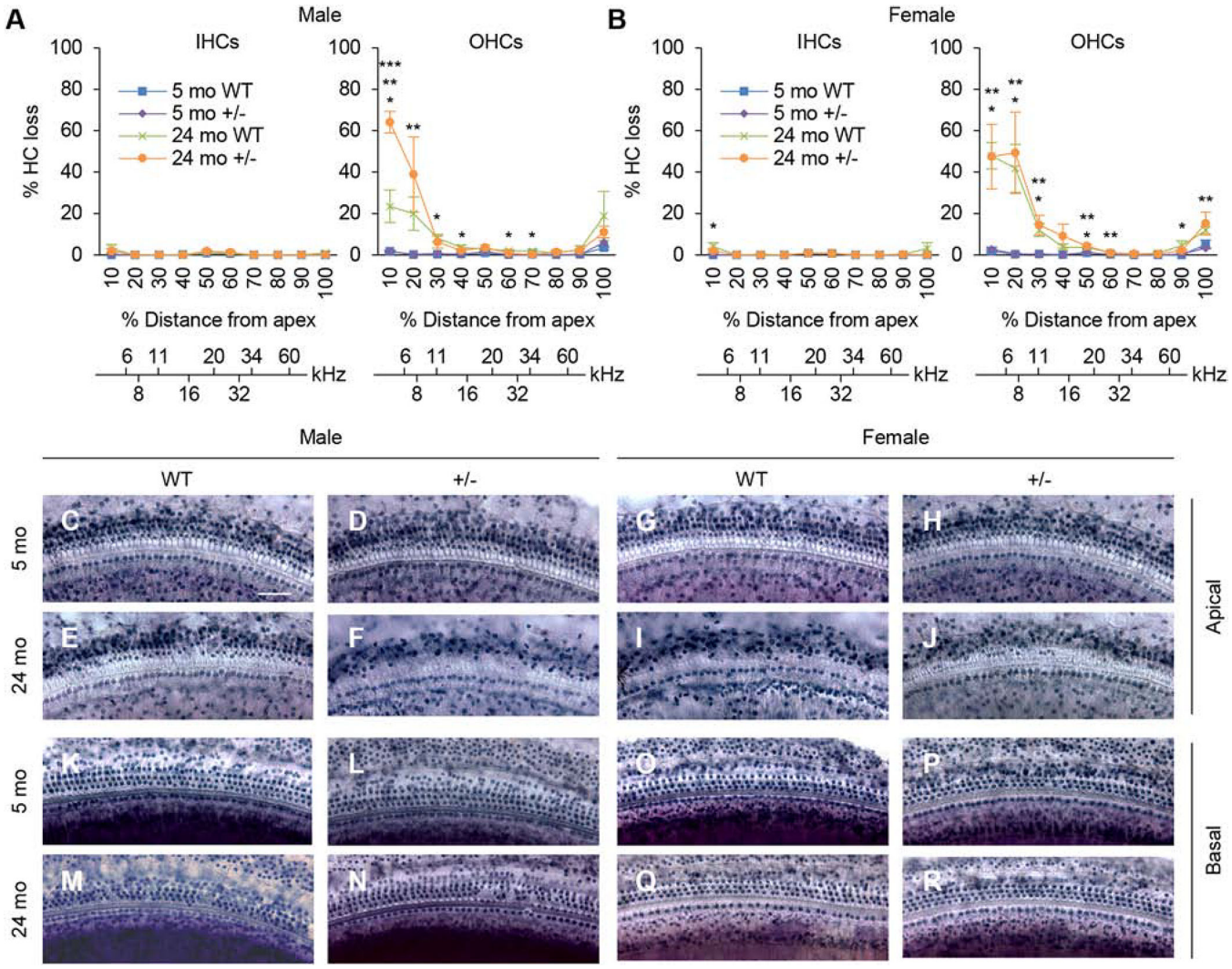

Fig. 4.

Effects of *Txn2* haplodeficiency on age-related degeneration of cochlear hair cells in mice. A-B: Cochleograms were recorded and averaged in the cochlear tissues from male (A) and female (B) WT and $Txn2^{+/-}$ mice at 3–5 (5) and 23–25 (24) months of age (N = 3–5). Graphs show percent loss of inner hair cells (IHCs) and outer hair cells (OHCs) as a function of percent distance from the apex. Lower x-axes show the frequency-place map for mouse cochlea. Data are shown as means ± SEM. *$p < 0.05$, 5 mo WT vs. 24 mo WT, **$p < 0.05$, 5 mo +/− vs. 24 mo +/−, ***$p < 0.05$, 24 mo WT vs. 24 mo +/−. C-R: Representative images of hair cells in the apical (C-J) and basal (K-R) turns of cochlear basilar membrane from male and female WT and $Txn2^{+/-}$ mice at 5 and 24 months of age. Scale bar = 50 μm.

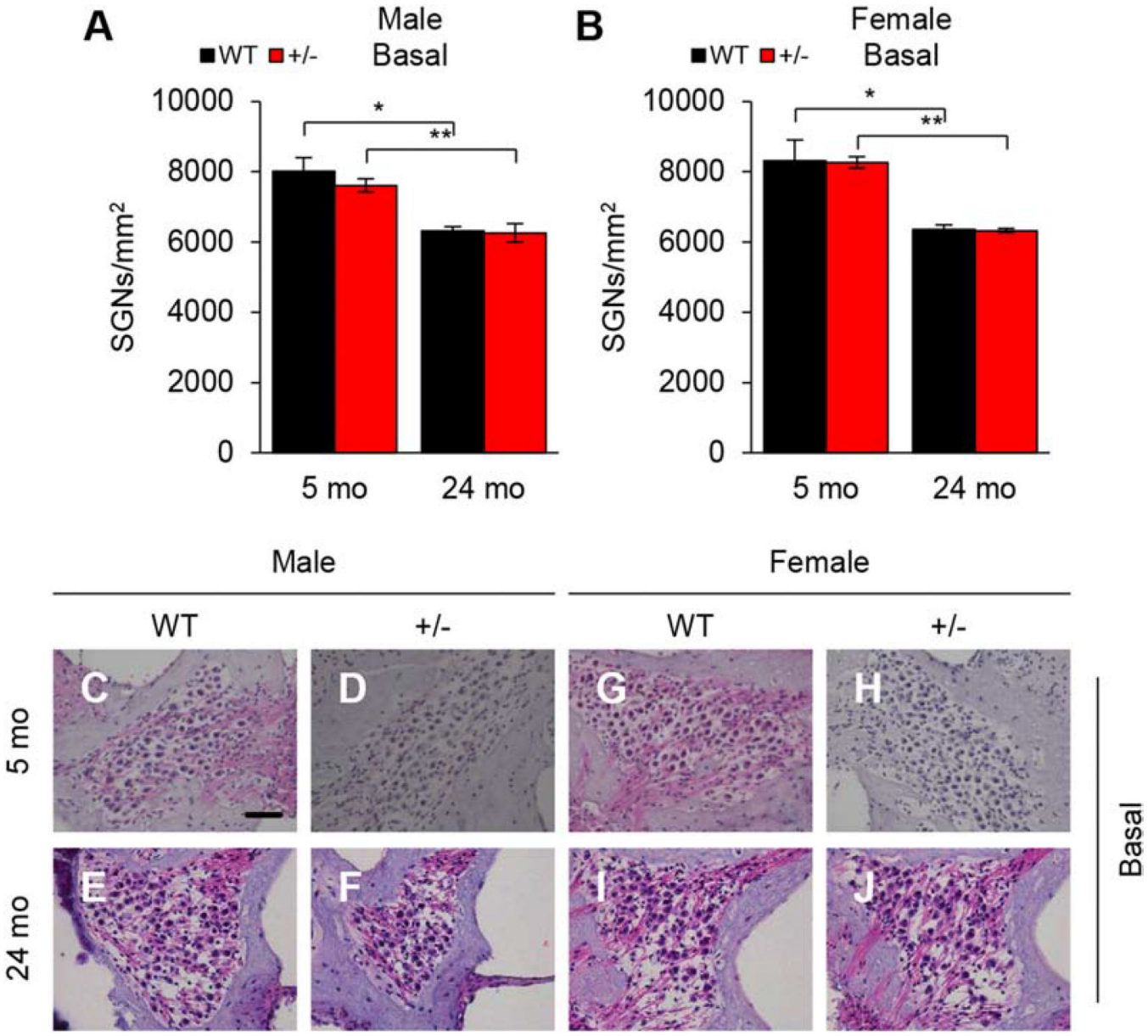

Fig. 5.

Effects of *Txn2* haplodeficiency on age-related degeneration of SGNs in mice. A-B: Spiral ganglion neurons (SGNs) were counted in the basal region of the cochlear tissues from male (A) and female (B) WT and $Txn2^{+/-}$ mice at 3–5 (5) and 23–25 (24) months of age ($N = 3$). Data are shown as means ± SEM. *$p < 0.05$, 5 mo WT vs. 24 mo WT, **$p < 0.05$, 5 mo +/− vs. 24 mo +/−. C-J: Representative images of SGNs in the basal cochlear tissues from male and female WT and $Txn2^{+/-}$ mice at 5 and 24 months of age. Scale bar = 20 μm.

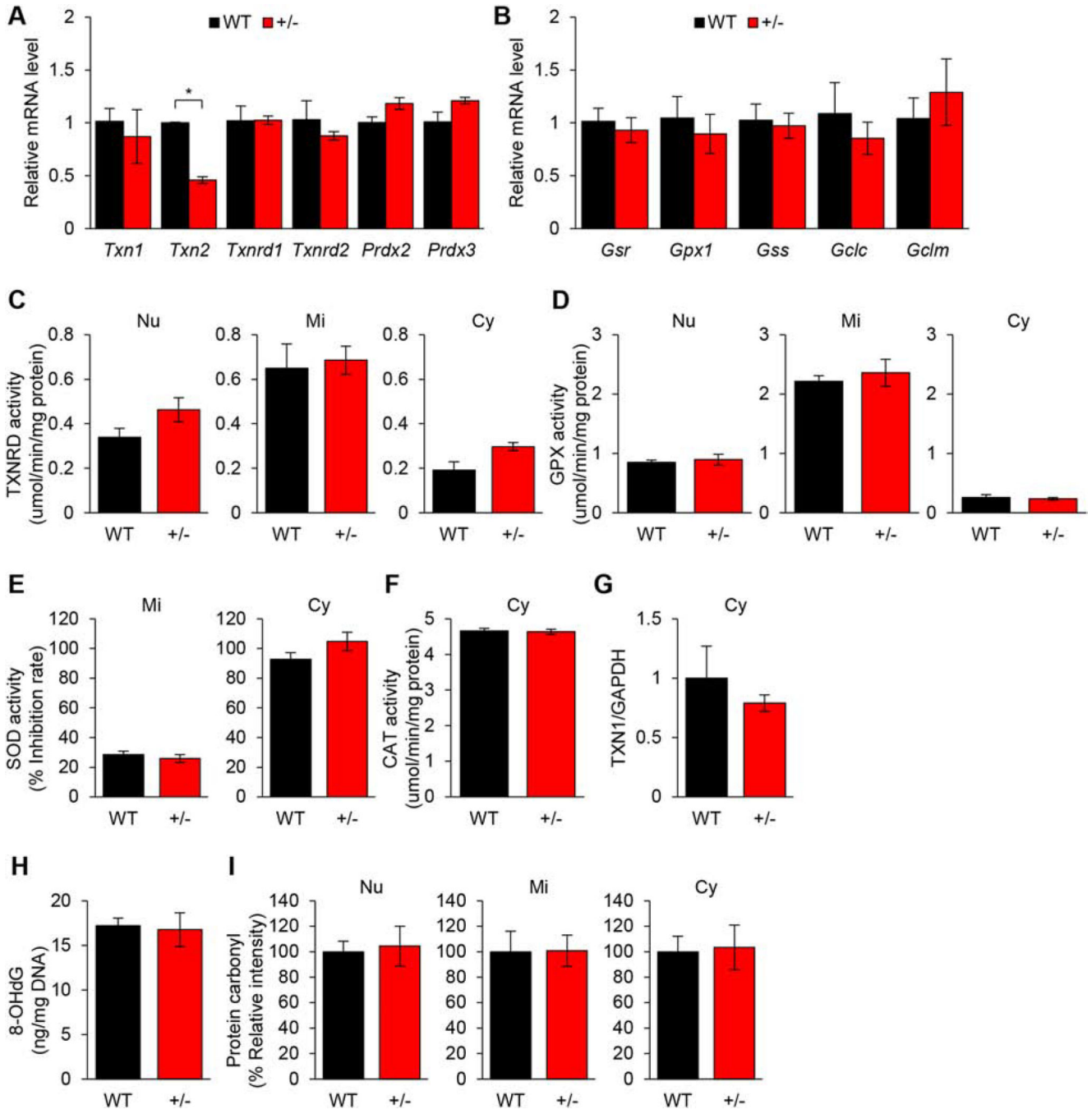

Fig. 6.

Effects of *Txn2* haplodeficiency on antioxidant defenses and oxidative damage in the inner ears of young mice. A-B: mRNA levels of genes involved in the thioredoxin (A) and glutathione (B) systems were measured in the inner ear tissues from 3–5 months old WT and $Txn2^{+/-}$ mice ($N = 3$). C-F: The activities of thioredoxin reductase (TXNRD) (C), glutathione peroxidase (GPX) (D), superoxide dismutase (SOD) (E), and catalase (CAT) (F) were measured in the nuclei (Nu), mitochondria (Mi), or cytosol (Cy) of the inner ear tissues from 3–5 months old WT and $Txn2^{+/-}$ mice ($N = 3$). (G) TXN1 protein levels were

measured in the cytosol (Cy) of the inner ear tissues from 3–5 months old WT and *Txn2*$^{+/-}$ mice ($N = 3$). GAPDH was used as a loading control. H-I: The levels of 8-oxoguanine (8-OHdG) (H) as an oxidative DNA damage marker and protein carbonyl (I) as an oxidative protein damage marker were measured in the Nu, Mi, or Cy of the inner ear tissues from 3–5 months old WT and *Txn2*$^{+/-}$ mice ($N = 3$). Data are shown as means ± SEM. *$p < 0.05$, WT vs. +/−.

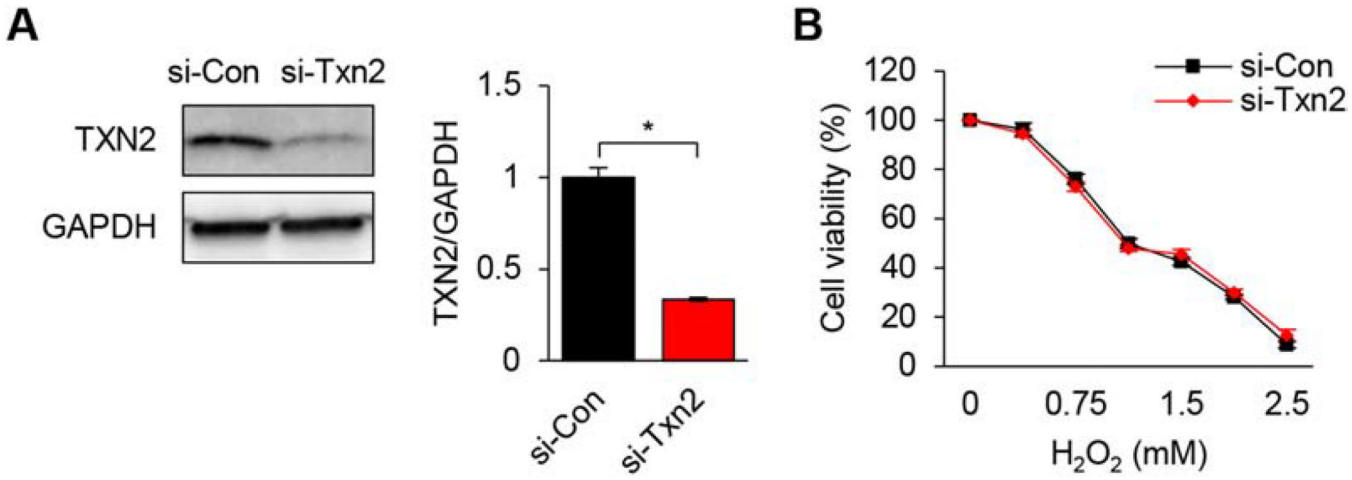

Fig. 7.

Effects of *Txn2* knockdown on cell viability in HEI-OC1 cells. (A) Western blot of TXN2 protein levels was performed in the whole cell lysates from controls and *Txn2* knockdown HEI-OC1 cells ($N = 3$). GAPDH was used as a loading control. (B) Cell viabilities were measured at 0, 0.5, 0.75, 1, 1.5, 2, and 2.5 mM H_2O_2 concentrations in controls and *Txn2* knockdown HEI-OC1 cells ($N = 4$). Data are shown as means ± SEM. *$p < 0.05$, si-Con vs. si-*Txn2*.

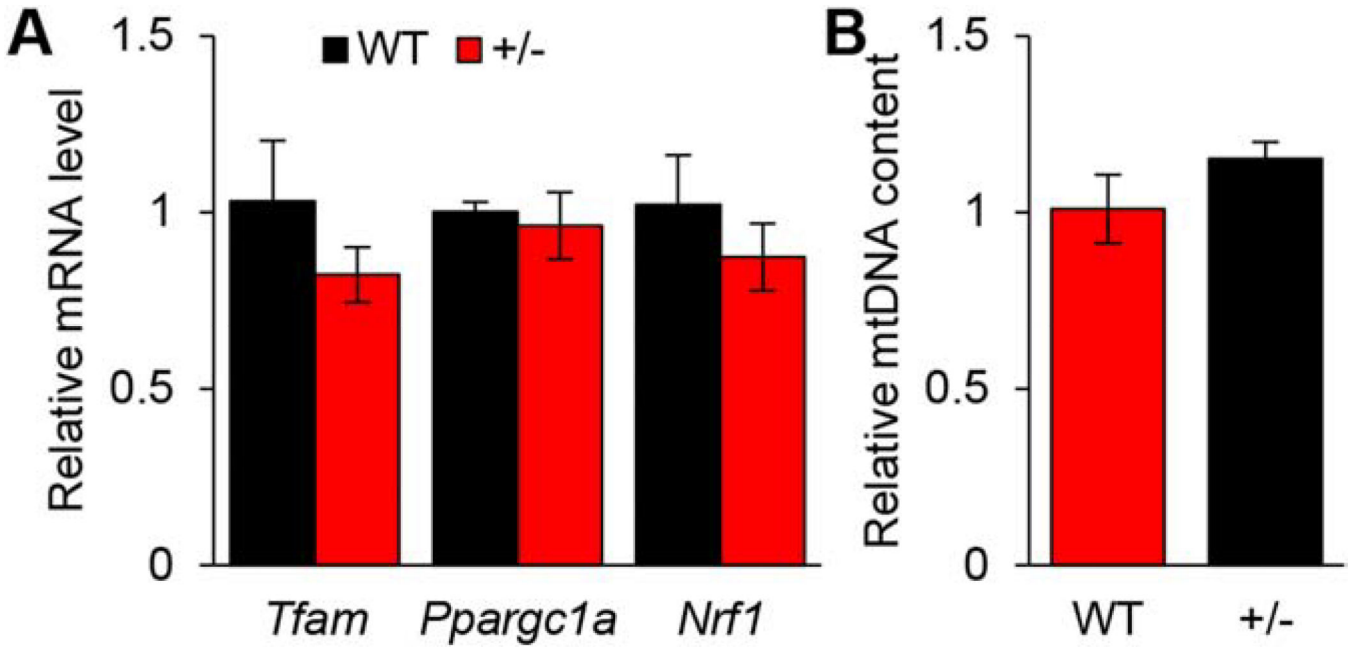

Fig. 8.

Effects of *Txn2* haplodeficiency on mitochondrial biogenesis in the inner ears of young mice. (A) mRNA levels of genes involved in mitochondrial biogenesis were measured in the inner ear tissues from 3–5 months old WT and $Txn2^{+/-}$ mice ($N = 3$). (B) Mitochondrial DNA (mtDNA) contents were measured in the inner ear tissues from 3–5 months old WT and $Txn2^{+/-}$ mice ($N = 3$). Data are shown as means ± SEM.